INSTITUTE OF PHYSICS PUBLISHING INVERSE PROBLEMS

Inverse Problems **20** (2004) 847–858 PII: S0266-5611(04)73511-X

A reconstruction formula and uniqueness of conductivity in MREIT using two internal current distributions

June-Yub Lee

Department of Mathematics, Ewha Womans University, Seoul 120–750, Korea

E-mail: jylee@math.ewha.ac.kr

Received 17 December 2003, in final form 4 March 2004
Published 26 March 2004
Online at stacks.iop.org/IP/20/847 (DOI: 10.1088/0266-5611/20/3/012)

Abstract

We consider a reconstruction formula for the internal conductivity and uniqueness of conductivity in magnetic resonance electrical impedance tomography (MREIT) which aims to reconstruct the conductivity distribution using internal current distribution. We provide a counter-example of uniqueness for a single measurement of current density with Neumann boundary data and show that at least two measurements are required unless Dirichlet boundary data are given. We present a reconstruction formula and a non-iterative reconstruction method using two internal current densities, which gives a unique conductivity distribution up to a constant factor even without any boundary measurement. The *curl-J* method is based on the fact that the distortion of the current density vector is induced by the gradient of conductivity orthogonal to the current flow and the fact that no MREIT method can detect the conductivity gradient parallel to the current flow direction directly. We demonstrate the feasibility of our method with several realistic numerical examples.

1. Introduction

A goal of electrical impedance tomography (EIT) is to recover the interior conductivity distribution σ satisfying the conductivity equation

$$\nabla \cdot (\sigma \nabla u) = 0 \qquad \text{in } \Omega \tag{1.1}$$

for electric potential u defined in a simply connected bounded Lipschitz domain Ω. Classical EIT attempts to solve this problem using the relationship between the injected current $\sigma \partial u/\partial \nu|_{\partial\Omega} = g$ and the corresponding boundary voltage $u|_{\partial\Omega} = f$ on $\partial\Omega$. Many theoretical and numerical approaches have been studied during the last couple of decades (see [3, 4] and

the references therein). However, no fully satisfactory numerical method exists due to the strong non-linearity and the highly ill-conditioned nature of the problem [13, 16].

A new imaging technique called magnetic resonance electrical impedance tomography (MREIT) significantly reduces the ill-conditioning of standard EIT by also using the internal current density as data. The current density data $\mathbf{J}$ is furnished by a recent current density imaging (CDI) technique [5, 6, 18, 19],

$$\mathbf{J} = \frac{1}{\mu}\nabla \times \mathbf{B} \qquad \text{in } \Omega \tag{1.2}$$

where the magnetic field $\mathbf{B}$ inside Ω can be obtained by magnetic resonance (MR) imaging. Some of the recent MREIT techniques directly utilize $\mathbf{B}$ instead of numerically differentiated $\mathbf{J}$ [2, 17, 20, 21]. We, however, focus on MREIT using $\mathbf{J}$ as input data and postpone detailed discussion on new $\mathbf{B}$-type MREIT or $\mathbf{B}$-MREIT techniques for subsequent papers. $\mathbf{J}$-type MREIT, or simply MREIT, is a problem to recover the conductivity distribution σ from some boundary measurements and the internal current density data

$$\mathbf{J} = -\sigma\nabla u \qquad \text{in } \Omega \tag{1.3}$$

which is divergence free, $\nabla \cdot \mathbf{J} = 0$.

Zhang [23] tried to find a conductivity σ distribution which satisfies Ohm's law (1.3) and best matches the measured boundary voltage difference $f(b) - f(a)$,

$$f(b) - f(a) = -\int_{C(a\to b)} \frac{1}{\sigma(x)}\mathbf{J}(x)\cdot \mathrm{d}\mathbf{l} \tag{1.4}$$

where $\mathbf{J}$ is given input data and $C(a \to b)$ is any path joining boundary points a and b. This minimization uses only a single measurement of $\mathbf{J}$ and Dirichlet data f, which can be classified as Dirichlet-type MREIT. Birgül *et al* [1] further extended this optimization idea to multiple Neumann measurements which provide internal current densities $\mathbf{J}_i$ and corresponding boundary current data g_i, but not voltage data. The current constrained voltage scaled reconstruction (CCVSR) algorithm starts with $\sigma^{(k=0)}$ and searches for an optimal $\sigma^{(k+1)}$ to minimize the difference between $-\sigma^{(k+1)}\nabla u_i^{(k)}$ and the given current density data $\mathbf{J}_i$,

$$\min_{\sigma} \sum_i \left\| \mathbf{J}_i + \sigma\nabla u_i^{(k)} \right\|^2_{L_2(\Omega)} \tag{1.5}$$

where $u_i^{(k)}$ satisfies $\nabla\cdot\sigma^{(k)}\nabla u_i^{(k)} = 0$ in Ω and $\sigma^{(k)}\frac{\partial}{\partial \nu}u_i^{(k)} = g_i$ on $\partial\Omega$. Both minimization methods could successfully remove the ill-conditioning of the standard EIT problems; however there is no clear way to find an optimizer σ other than iterating with previous guesses.

The first attempt based on the partial differential equation (1.1), not just Ohm's law (1.3), to reconstruct the conductivity distribution σ was made by Kwon *et al* in [12]. Combining (1.1) and (1.3), they derived a non-linear partial differential equation for u with given current data $|\mathbf{J}|$,

$$\nabla\cdot\left(\frac{|\mathbf{J}|}{|\nabla u|}\nabla u\right) = 0 \qquad \text{in } \Omega. \tag{1.6}$$

The conductivity σ can be easily obtained once this non-linear equation is solved; however the PDE cannot be solved using a single measurement of $|\mathbf{J}|$ due to non-uniqueness [9]. So they use two measurements of the *magnitude* of interior current density $|\mathbf{J}_1|$ and $|\mathbf{J}_2|$ and try to solve the coupled non-linear PDE,

$$\nabla\cdot\left(\frac{|\mathbf{J}_i|}{|\nabla u_i|}\nabla u_i\right) = 0 \quad \text{in } \Omega \qquad i = 1, 2 \tag{1.7}$$

$$\frac{|\mathbf{J}_1|}{|\nabla u_1|} = \frac{|\mathbf{J}_2|}{|\nabla u_2|} \qquad \text{in } \Omega \tag{1.8}$$

$$\frac{|\mathbf{J}_i|}{|\nabla u_i|}\frac{\partial u_i}{\partial \nu} = g_i \qquad \text{on } \partial\Omega \qquad i = 1, 2. \tag{1.9}$$

The coupled PDE guarantees the uniqueness of σ up to a constant and can be solved iteratively where each iteration is accomplished by the alternative substitution of intermediate conductivity distribution [10]. The *J-substitution* algorithm also shows good experimental results [8, 14]. However, the algorithm needs to solve the non-linear partial differential equation (1.6) iteratively thus strongly relying on a fast and accurate forward numerical solver.

Our main goal in this paper is to present a direct reconstruction formula for σ which does not require an iterative forward solver. A direct solver is also able to reconstruct the conductivity σ in a region of interest (ROI) even when there is experimental difficulty in obtaining necessary information outside the field of view. There were a couple of previous attempts to find conductivity directly: the equipotential line method by Kwon *et al* [11] and the first-order hyperbolic PDE approach by Ider *et al* [7]. We briefly mention two closely related approaches before presenting our new *curl-J* reconstruction method.

Kwon *et al* [11] observed that the MREIT problem has nothing to do with the complicated non-linear partial differential equation (1.6), but the inverse problem can be solved explicitly using the first-order differential equation (1.3),

$$-\sigma\nabla u = \mathbf{J} \qquad \text{in } \Omega \qquad \text{and} \qquad u = f \qquad \text{on } \partial\Omega \tag{1.10}$$

where $(\mathbf{J}, f)$ are the given data for Dirichlet-MREIT. The equipotential line method computes all the equipotential lines $X(s)$ by solving the ordinary differential equation with the boundary data f,

$$X'(s) = \left(\frac{\nabla u}{|\nabla u|}\right)^{\perp} \tag{1.11}$$

where $(\cdot)^{\perp}$ denotes the anticlockwise right angle rotation. Then the conductivity distribution can be calculated using the computed $|\nabla u|$ and the given magnitude information $|\mathbf{J}|$, $\sigma = |\mathbf{J}|/|\nabla u|$. This idea of a system of first-order ordinary differential equations can be extended to Neumann-type MREIT using two current densities $\mathbf{J}_1$ and $\mathbf{J}_2$ wherever f information is not available [7]. By taking the curl of Ohm's law (1.3), we get

$$-\nabla\sigma \times \nabla u = \nabla \ln\sigma \times \mathbf{J} = \nabla \times \mathbf{J} \tag{1.12}$$

and we obtain a first-order hyperbolic partial differential equation for σ,

$$\mathbf{J}_d \cdot \nabla \ln\sigma = \big(\nabla \times \mathbf{J}\big) \cdot \mathbf{d} \tag{1.13}$$

where $\mathbf{J}_d := \mathbf{J} \times \mathbf{d}$ and $\big(\nabla \times \mathbf{J}\big) \cdot \mathbf{d}$ are given data for any given directional vector $\mathbf{d}$ in $\mathbf{R}^3$. This hyperbolic equation for σ (1.13) can be solved explicitly using two current densities $\mathbf{J}_1$ and $\mathbf{J}_2$ by the method of characteristics, integrating over a Cartesian grid, and inversion of a finite difference matrix by Ider *et al* [7].

In this paper, we present a formula to solve the *curl-J* identity (1.12) directly without solving any partial differential equation. In section 2, we comment on the uniqueness of conductivity in Dirichlet-MREIT and non-uniqueness of Neumann-MREIT with a single measurement. In section 3, we describe our *curl-J* reconstruction formula and a non-iterative numerical method using two internal current distributions $\mathbf{J}_1$ and $\mathbf{J}_2$ without any boundary condition. In section 4, we present various numerical examples and discuss the convergence of our implementation and the stability of the algorithm under noisy input data.

2. Uniqueness of Dirichlet- and Neumann-type MREIT

Let $\Omega \subset \mathbf{R}^3$ be a simply connected bounded domain with $\mathcal{C}^2$ boundary and let the conductivity distribution $\sigma \in \mathcal{C}^1(\Omega)$ satisfy $0 < \sigma(x) < \infty$ for all $x \in \bar{\Omega}$. Then the conductivity equation $\nabla \cdot (\sigma \nabla u) = 0$ in Ω has a unique solution given either Dirichlet boundary condition $u = f$ or Neumann boundary condition $\sigma \frac{\partial u}{\partial \nu} = g$ on $\partial\Omega$ with a trivial normalization such as $\int_{\partial\Omega} u = 0$.

The goal of MREIT is to reconstruct the conductivity σ using the internal current density $\mathbf{J} = -\sigma \nabla u$ which can be obtained by the CDI technique. The Dirichlet-type MREIT problem with non-vanishing divergence-free current density $\mathbf{J}$ and continuous Dirichlet boundary condition f

$$\mathbf{J} = -\sigma \nabla u \text{ in } \Omega \qquad \text{and} \qquad u = f \text{ on } \partial\Omega \tag{2.1}$$

has a unique solution of conductivity and potential [11]. The proof is based on the equipotential line method and it can be easily extended to the case where boundary conductivity is given instead of boundary potential. However, it is more difficult to accurately measure boundary conductivity with surface current density or boundary potential than Neumann boundary data on $\partial\Omega$.

Therefore, it is an important question whether we can reconstruct conductivity uniquely using only $\mathbf{J}$ in Ω and g on $\partial\Omega$. Unfortunately, Neumann-type MREIT with

$$\mathbf{J} = -\sigma \nabla u \text{ in } \Omega \qquad \text{and} \qquad g = \sigma \frac{\partial u}{\partial \nu} \text{ on } \partial\Omega \tag{2.2}$$

has non-uniqueness examples [9]. Furthermore, there exist infinitely many solutions of the Neumann-type MREIT problem. Suppose σ_u is a conductivity distribution with corresponding u satisfying

$$\nabla \cdot (\sigma_u \nabla u)(x) = 0. \tag{2.3}$$

Then for any strictly-increasing function $V \in \mathcal{C}^1(\mathbf{R})$,

$$v(x) = V(u(x)) \tag{2.4}$$

$$\sigma_v(x) = \frac{\sigma_u(x)}{V'(u(x))} \tag{2.5}$$

satisfies $\nabla \cdot (\sigma_v \nabla v)(x) = 0$ with the same current density $\mathbf{J} = -\sigma_u \nabla u = -\sigma_v \nabla v$ in Ω and Neumann boundary condition $g = \sigma_u \frac{\partial u}{\partial \nu} = \sigma_v \frac{\partial v}{\partial \nu}$ on $\partial\Omega$.

We conclude this section by commenting that a single current density measurement, even with Neumann boundary data, is not enough to reconstruct conductivity distribution uniquely and our goal of this paper is to develop a fast and efficient non-iterative reconstruction scheme with two current density measurements.

3. A reconstruction formula

In this section, we assume that the conductive media in Ω are isotopic and there is no internal current source so that current density vector field $\mathbf{J} = -\sigma \nabla u$ is divergence free. By taking the curl of $\mathbf{J}$, we get the following *curl-J* identity:

$$-\nabla\sigma \times \nabla u = \nabla \times \mathbf{J}, \tag{3.1}$$

$$\frac{\nabla\sigma}{\sigma} \times \mathbf{J} = \nabla \times \mathbf{J}. \tag{3.2}$$

The Helmholtz theorem states that a divergence-free vector field can be reconstructed from its curl field so $\nabla \times \mathbf{J}$ contains the same information as $\mathbf{J}$. Therefore, neither $\nabla \times \mathbf{J}$ nor $\mathbf{J}$ can provide information about conductivity changes $\frac{\nabla\sigma}{\sigma}$ parallel to $\mathbf{J}$. This is the reason why the uniqueness result from a single measurement requires extra information along a current field line.

Now suppose that we have two current density profiles, $\mathbf{J}_1(x)$ and $\mathbf{J}_2(x)$ in Ω, whose cross product is non-vanishing $\mathbf{J}_1(x) \times \mathbf{J}_2(x) \neq 0$. This non-vanishing cross-product condition can easily be obtained in most experimental environments (see lemma 4.2 in [9]). Then from (3.2), the conductivity $\sigma(x)$ satisfies the following two equations simultaneously,

$$\frac{\nabla\sigma}{\sigma}(x) \times \mathbf{J}_1(x) = \nabla \times \mathbf{J}_1(x) \tag{3.3}$$

$$\frac{\nabla\sigma}{\sigma}(x) \times \mathbf{J}_2(x) = \nabla \times \mathbf{J}_2(x). \tag{3.4}$$

In order to make a representation formula for $\frac{\nabla\sigma}{\sigma}(x)$ using $\nabla \times \mathbf{J}_1(x)$ and $\nabla \times \mathbf{J}_2(x)$, we choose

$$A(x) := \frac{\mathbf{J}_1 + \mathbf{J}_2}{2} \qquad B(x) := \frac{\mathbf{J}_2 - \mathbf{J}_1}{2} \qquad C(x) := \mathbf{J}_1 \times \mathbf{J}_2 \tag{3.5}$$

as three independent basis vector sets in $\mathbf{R}^3$. Using these three basis vectors, the gradient of conductivity can be represented as

$$\frac{\nabla\sigma}{\sigma}(x) = a(x)A(x) + b(x)B(x) + c(x)C(x) \tag{3.6}$$

and by multiplying $\mathbf{J}_1(x)$ and $\mathbf{J}_2(x)$, we get

$$\frac{\nabla\sigma}{\sigma} \times \mathbf{J}_1(x) = \frac{a+b}{2}(\mathbf{J}_2 \times \mathbf{J}_1) + c\left((\mathbf{J}_1 \cdot \mathbf{J}_1)\mathbf{J}_2 - (\mathbf{J}_1 \cdot \mathbf{J}_2)\mathbf{J}_1\right) \tag{3.7}$$

$$\frac{\nabla\sigma}{\sigma} \times \mathbf{J}_2(x) = \frac{a-b}{2}(\mathbf{J}_1 \times \mathbf{J}_2) + c\left((\mathbf{J}_1 \cdot \mathbf{J}_2)\mathbf{J}_2 - (\mathbf{J}_2 \cdot \mathbf{J}_2)\mathbf{J}_1\right). \tag{3.8}$$

Combining these equations with (3.3) and (3.4), we can derive the *curl-J* reconstruction formula

$$\frac{\nabla\sigma}{\sigma} = a(x)\frac{\mathbf{J}_1 + \mathbf{J}_2}{2} + b(x)\frac{\mathbf{J}_2 - \mathbf{J}_1}{2} + c(x)(\mathbf{J}_1 \times \mathbf{J}_2) \tag{3.9}$$

where

$$a(x) = \frac{\mathbf{J}_1 \times \mathbf{J}_2}{|\mathbf{J}_1 \times \mathbf{J}_2|^2} \cdot (\nabla \times \mathbf{J}_2 - \nabla \times \mathbf{J}_1) \tag{3.10}$$

$$b(x) = \frac{\mathbf{J}_2 \times \mathbf{J}_1}{|\mathbf{J}_1 \times \mathbf{J}_2|^2} \cdot (\nabla \times \mathbf{J}_1 + \nabla \times \mathbf{J}_2) \tag{3.11}$$

$$c(x) = \frac{\mathbf{J}_2 \cdot \nabla \times \mathbf{J}_1}{|\mathbf{J}_1 \times \mathbf{J}_2|^2} = -\frac{\mathbf{J}_1 \cdot \nabla \times \mathbf{J}_2}{|\mathbf{J}_1 \times \mathbf{J}_2|^2}. \tag{3.12}$$

Once the conductivity gradient field $\mathbf{F}(x) := \frac{\nabla\sigma}{\sigma}(x)$ is obtained

$$\mathbf{F}_{[\mathbf{J}_1, \mathbf{J}_2, \nabla\times\mathbf{J}_1, \nabla\times\mathbf{J}_2]}(x) = a(x)A(x) + b(x)B(x) + c(x)C(x) \tag{3.13}$$

from the two physical measurements of $\mathbf{J}_1, \mathbf{J}_2$ in Ω, the conductivity distribution $\sigma(x)$ can be computed uniquely up to a constant,

$$\sigma(x) = \sigma(x_0) \exp\left(\int_{C(x_0 \to x)} \mathbf{F}(y) \cdot \mathrm{d}y\right) \tag{3.14}$$

where $C(x_0 \to x)$ is any path in Ω from x_0 to x. Here, $\sigma(x_0)$ might be a known conductivity value at x_0 or could be derived from a single voltage measurement [7, 8]. The formula will give a unique result independent of the path joining x_0 to x since the vector field $\mathbf{F}(x)$ is a gradient field when there is no noise on $\mathbf{J}_1$ and $\mathbf{J}_2$ or $\nabla \times \mathbf{J}_1$ and $\nabla \times \mathbf{J}_2$.

When there exists some noise in the data, a conductivity profile can be found in the least squares sense using the over-determined gradient field $\mathbf{F}(x)$,

$$\sigma(x) = \sigma(x_0) \exp(s(x) - s(x_0)) \qquad \text{where} \quad \min_s \|\nabla s - \mathbf{F}\|_{L_2(\Omega)}. \tag{3.15}$$

We choose rectangular bilinear elements $\{\phi_j\}$ as a basis for s, $s(x) = \sum_{j=1}^{N} s_j \phi_j(x)$ and solve a Galerkin-type finite element minimization equation,

$$\sum_{j=1}^{N} s_j \int_\Omega \nabla\phi_j \cdot \nabla\phi_i \, \mathrm{d}x = \int_\Omega \mathbf{F} \cdot \nabla\phi_i \, \mathrm{d}x \qquad \text{for} \quad i = 1, \ldots, N \tag{3.16}$$

with the constraint $s(x_0) = \log(\sigma(x_0))$ at any given point x_0.

We conclude this section by mentioning that the *curl-J* algorithm is the first explicit reconstruction method for Neumann-type MREIT. There is no iterative forward solver for optimization nor partial differential equation to solve. The *curl-J* reconstruction formula (3.13) is explicit and the corresponding conductivity can also be computed explicitly using the path integration of $\mathbf{F}$ in (3.14). A finite element minimization to find s in (3.15) is merely one of many possible denoising techniques for noisy $\mathbf{J}$ data.

4. Numerical examples

The *curl-J* method described in the previous section has been implemented in Fortran 77. In principle, there is no difference between two- and three-dimensional algorithms but for the sake of simplicity we demonstrate only two-dimensional examples where the solutions do not depend on z. In this section, we present three numerical examples. The first example demonstrates numerical accuracy and convergence order of the implementation, the second shows robustness and stability of the method even with noisy data and the third presents practical feasibility of the algorithm for realistic situations. The computational cost for computation of $\mathbf{F}$ in (3.13) on an $n \times n$ grid is only $O(n^2)$ and is dominated by the $O(n^3)$ cost of finding finite element minimization solution s in (3.16). The computation itself takes around 1.2 s for a 128×128 grid and 10 s for a 256×256 grid under 866 MHz Pentium III CPU without applying any serious optimization techniques.

Example 1 (order of convergence). The first example contains rectangular and elliptic inclusions in a rectangular homogeneous medium of size $[-1, 1]^2$. Each of the inclusions has constant conductivity from 10^{-3} to 10^3 and the conductivity near the inclusion boundary sharply but continuously changes to background conductivity with a $\frac{1}{200}$ length scale. We solve the conductivity equation (1.1) twice, once with current flowing from the left to the right boundary and second with current flowing from the bottom to the top using a standard second-order finite element method on a 512×512 grid in order to get two current densities $\mathbf{J}_1$ and $\mathbf{J}_2$ for this experiment.

Figure 1 shows the conductivity distribution σ and the current density profile $\mathbf{J}_1$ and $\mathbf{J}_2$. The rightmost figure shows the angle between $\mathbf{J}_1$ and $\mathbf{J}_2$. Current tends to flow towards the nearby conductor, therefore the angle between two current directions remains almost the same near highly conductive inclusions surrounded by a poor conductor. Even though $\mathbf{J}_1 \times \mathbf{J}_2 \neq 0$ mathematically [9], there are several regions where the two directions are nearly parallel.

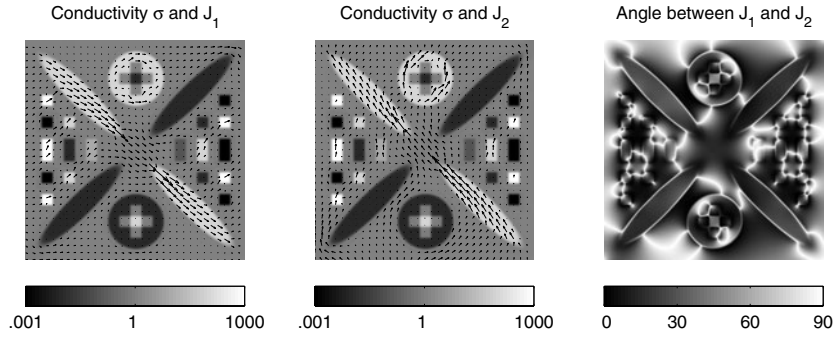

Figure 1. Conductivity distribution σ and current density profiles of $\mathbf{J}_1$ and $\mathbf{J}_2$ for example 1. The rightmost figure shows the angle between $\mathbf{J}_1$ and $\mathbf{J}_2$ with white indicating a region of orthogonality.

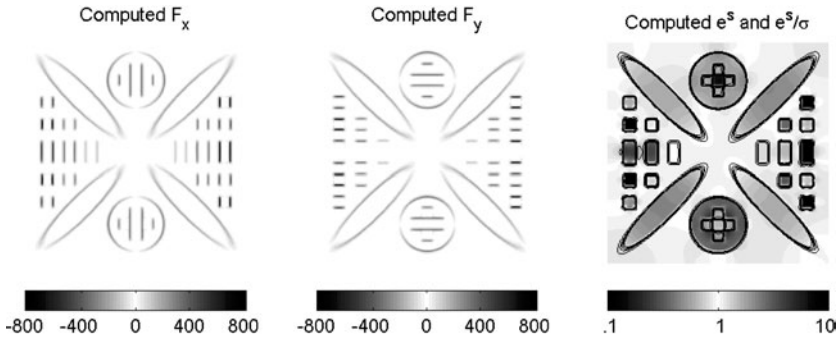

Figure 2. Computed gradient field $\mathbf{F}$ for example 1. Contour lines in the rightmost figure show the reconstructed $\log_{10}\sigma$ on 256×256 grid and grey shading shows the ratio of the reconstruction solution to the original.

The effects of parallel flow direction due to noise or computational error will be discussed later.

Figure 2 shows the computational results for x and y components of $\mathbf{F}$ and $\sigma = \mathrm{e}^s$ on a 256×256 grid. We take down-sampled 256×256 $\mathbf{J}_1$ and $\mathbf{J}_2$ data from those on a 512×512 grid in figure 1, then apply a second-order finite difference to compute $\mathbf{F}$ using (3.10)–(3.12) followed by a second-order finite element minimization for s using (3.16). Relative L_2 computational error defined by $E_s := \frac{\|s-\log(\sigma)\|_2}{\|\log(\sigma)\|_2}$ is 0.23 for this computation and grey shading in the rightmost figure shows the local error in terms of the ratio of computed to true conductivity. It indicates that higher error occurs near poorly conductive regions surrounded by good conductors, which is a natural phenomenon in any type of inverse conductivity reconstruction algorithm.

We reconstruct conductivity on four different grids in order to check the order of accuracy of the implementation. All four sets of current density data $\mathbf{J}_1$ and $\mathbf{J}_2$ are obtained by down-sampling the same forward solution on 512×512 to reduce the effect of the forward solver error. Figure 3 shows the reconstructed solutions on 128×128 and on 512×512 whose relative L_2 errors of s are $E_s = 1.4$ and $E_s = 0.05$, respectively. The rightmost plot shows that the implementation is of second order. The actual error value depends on the range of conductivity and the smoothness of current density. Developing a higher order method even

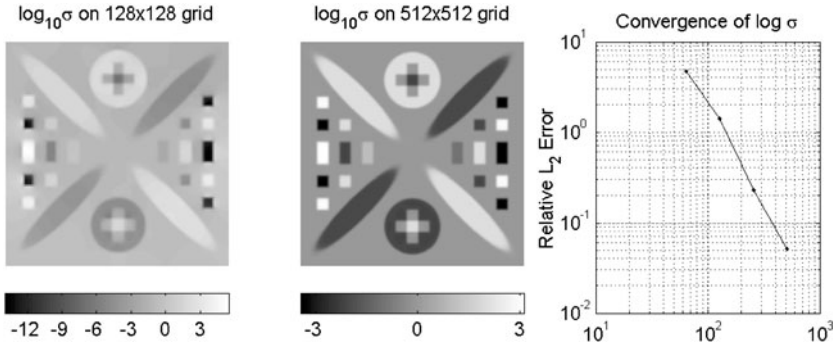

Figure 3. Reconstructed σ on 128×128 and 512×512 grids. The rightmost plot shows relative L_2-error convergence of $s = \log \sigma$ in terms of the number of grid points.

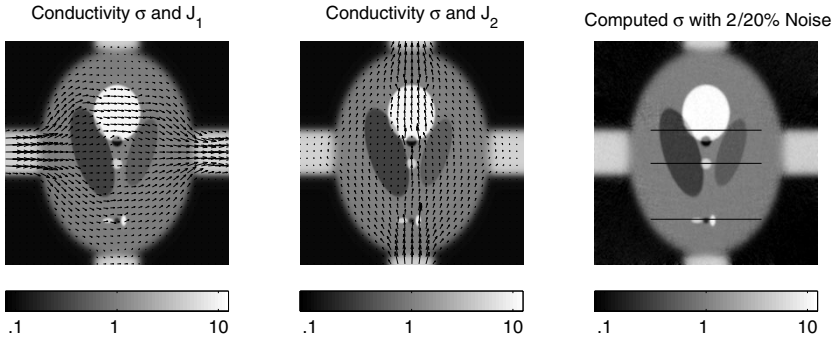

Figure 4. Conductivity distribution σ and current density profile of $\mathbf{J}_1$ and $\mathbf{J}_2$ for example 2. The rightmost figure shows the reconstructed conductivity distribution on a 256×256 grid with 2% additive and 20% multiplicative noise.

with discontinuous current density is a rather technical job but an important future task for real applications.

Example 2 (stability under noise). The second example checks stability of the algorithm under noisy input data using a phantom shown in figure 4. The phantom has eight inclusions whose constant conductivity values are between 0.1 and 10 inside but sharply change to 1 near the boundaries with a $\frac{1}{500}$ length scale. Four highly conductive limbs, coined as recessed electrodes in [15], provide two different types of current injections and suctions.

Current density data $\mathbf{J}_1$ and $\mathbf{J}_2$ on a 256×256 grid are obtained using a second-order FEM solver. Then the data are mixed with additive and multiplicative noise. Multiplicative noise is linearly proportional to $\mathbf{J}(x, y)$ like signal measurement error while additive noise is independent of local amplitude like white background noise. For additive noise level $\text{noise}_{\text{add}}$ and multiplicative noise level $\text{noise}_{\text{mul}}$, computational input data are given as follows,

$$\mathbf{J}_{\text{noisy}}(x, y) = \mathbf{J} + \text{noise}_{\text{add}}\left(\epsilon_x^a, \epsilon_y^a\right)\|\mathbf{J}\|_2 + \text{noise}_{\text{mul}}\left(\epsilon_x^m \mathbf{J}_x, \epsilon_y^m \mathbf{J}_y\right) \tag{4.1}$$

where $\epsilon_x^a, \epsilon_y^a, \epsilon_x^m$ and ϵ_y^m are four independent random variables uniformly distributed on $[-1, 1]$.

The rightmost picture in figure 4 shows the computational result for σ with 2% additive and 20% multiplicative noise, which gives 7.5% relative L_2 error in s, $E_s = 0.075$. The conductivity on the three marked lines in the figure has been drawn in three graphs in figure 5.

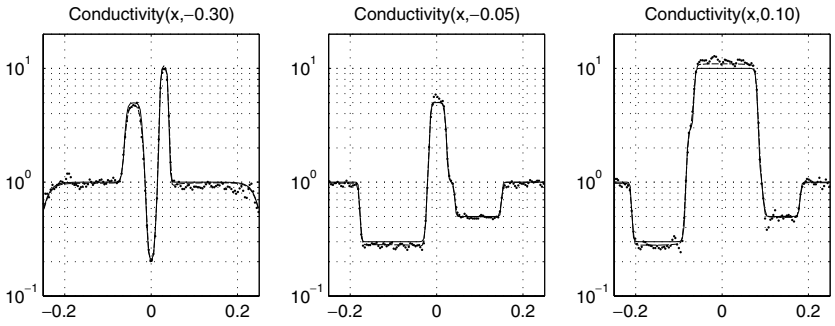

Figure 5. Reconstructed conductivity on the three marked lines in figure 4 for example 2. Solid lines are used for the original conductivity, dashed lines for the computational result without noise and dotted lines with 2% additive and 20% multiplicative noise.

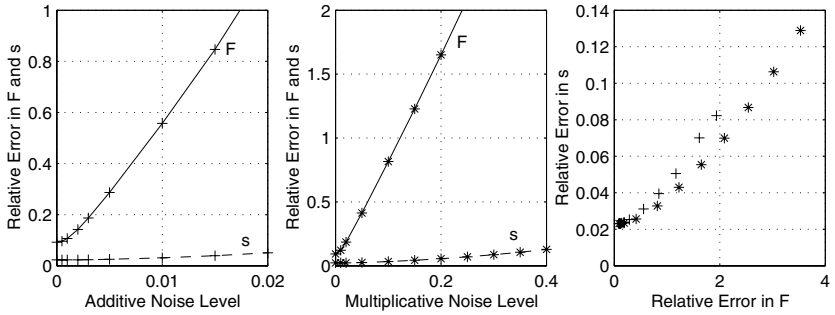

Figure 6. Relative **F**-reconstruction error with additive and multiplicative noise. Solid lines for L_2-relative error in **F** and dashed lines for error in s. markers + for additive noise and * for multiplicative noise. The rightmost plot shows the relationship between s-reconstruction error and **F**-reconstruction error.

The solid lines are used for the original conductivity, the dashed lines for the reconstruction without noise and the dotted lines for the computational result shown in figure 4 with 2/20% noise.

In order to check the stability of the algorithm in the presence of noise, we increase the additive noise level from 0 to 2% with 0% multiplicative noise. The leftmost graph in figure 6 shows the L_2-relative errors in **F** and s, compared to the original values, E_F and E_s are proportional to the noise level. The middle graph shows the same errors when the multiplicative noise level varies from 0 to 40% with 0 additive noise. These experiments demonstrate that the reconstruction errors are linearly proportional to the noise level, thus the algorithm is linearly stable to the noise. There are two reasons why reconstruction error for **F** is not zero even without any noise. The first one is that our simulation data $\mathbf{J}_1$ and $\mathbf{J}_2$ on 256×256 already contain discretization error from a second-order finite element forward solver. The second reason is that we use a second-order finite difference scheme to compute $\nabla \times \mathbf{J}$ in (3.10)–(3.12). The rightmost graph in figure 6 shows the relationship between error in **F** and error in s from both experiments. It shows that the overall reconstruction error for s is linearly proportional to the error level of **F** regardless of the type of error source. Again the second-order Galerkin-type minimization method has discretization error and does not give a perfect s even with error-free **F**.

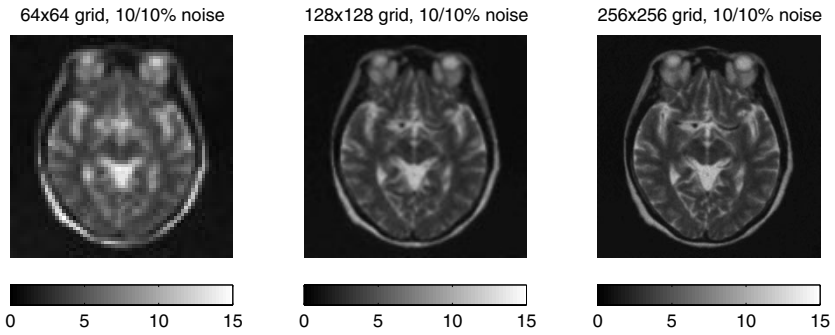

Figure 7. Reconstructed conductivity distribution with 10% additive and 10% multiplicative noise on 64×64, 128×128 and 256×256 grids.

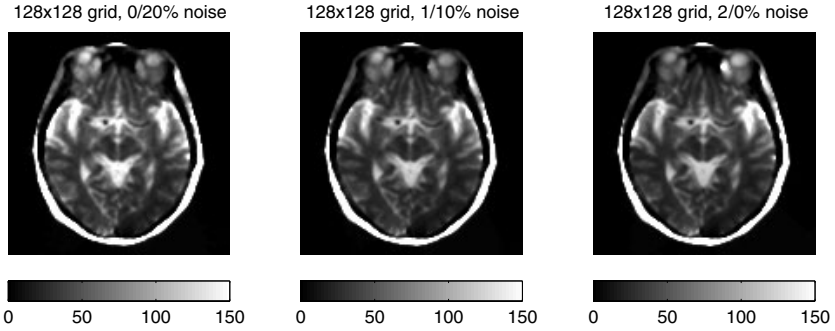

Figure 8. Reconstructed conductivity distribution on a 128×128 grid with various noise levels.

The actual size of the relative error for $\mathbf{F}$ depends on many factors such as current density profile, the numerical method used to compute the curl of $\mathbf{J}$ and the discritization number. However, the algorithm stably computes s in the presence of up to 40% multiplicative noise in most cases regardless of the error size in $\mathbf{F}$, which suggests that the minimization solution s can be obtained as long as the current flow direction is preserved. Another interesting point is that errors in $\mathbf{F}$ or s are around 10 times larger for additive noise than for the same level of multiplicative noise. The ratio 10 depends largely on the contrast ratio which is the rough ratio between the largest to average or the average to the smallest conductivity. In this examples, the current density in a poor conductor is about 10 times smaller than average, therefore it is 10 times more vulnerable to changes in local flow direction change.

Example 3 (human head phantom). *In vivo* electrical conductivity for the human body is not yet available, so we simply assign conductivity values proportional to the intensity of a 256×256 human head MRI image. The conductivity for the first simulation ranges from 1 to 10 and is discontinuous, unlike the previous examples. Two current density vectors $\mathbf{J}_1$ and $\mathbf{J}_2$ are obtained from the same finite element solver used for example 1 and then 10% additive and 10% multiplicative noise are added. Figure 7 shows the reconstructed conductivity on 64×64, 128×128 and 256×256 under-sampled grids whose L_2-relative errors in s, E_s are 37.3%, 15.6% and 8.8%, respectively. The algorithm reconstructs the discontinuous conductivity distribution reasonably well even on a 64×64 grid with 10/10% noise level. The reconstructed image on a 256×256 grid is not easily distinguishable from the original.

The conductivity for the second simulation ranges from 1 to 100. Figure 8 shows the reconstructed conductivity on a 128×128 grid with various noise levels. The reconstruction errors E_s are 48.5%, 48.9%, 52.0% with 0/20%, 1/10%, 2/0% additive/multiplicative noise, respectively. The reconstruction quality is quite similar but worse than the result for a 128×128 grid with 10/10% noise. We could infer from this simulation that 1% additive noise has a similar effect as 10% multiplicative noise in the reconstruction of conductivity with contrast ratio around 10.

5. Conclusion

We implemented a direct and stable numerical method for MREIT using two current density profiles based on the *curl-J* identity (3.2) and the corresponding *curl-J* reconstruction formula (3.13). The algorithm is based on a reconstruction formula, so it does not require an iterative forward solver and the result is linearly stable with respect to the noise level.

Example 2 and figure 6 show that the error of $\mathbf{F}$ in the reconstruction formula (3.13) is significantly higher than minimization solution s although both $\mathbf{F}$ and s are linearly stable with respect to the noise level. In particular, error in $\mathbf{F}$ may be locally high when $\mathbf{J}_1 \times \mathbf{J}_2 \approx 0$; however this local error peak can be significantly reduced by the minimization procedure (3.16). A fundamental requirement for the reconstruction procedure in a noisy environment is preservation of global current flow direction $\mathbf{F}$ and the algorithm could provide a good image even with 40–50% multiplicative noise. The effect of additive noise is much stronger in poorer conducting regions and a key factor to the reconstruction image quality is the contrast ratio times the additive noise level. The resistivity of the human body is below 100 Ω cm for body fluid and above 10 000 Ω cm for bone, so the signal-to-noise ratio (SNR) for $\mathbf{J}$ should be around 100 in order to apply this reconstruction algorithm to such a sample with contrast ratio around 10.

It is current state-of-the-art in MRCDI technique to obtain current density data $\mathbf{J}$ with SNR higher than 100, so making a robust and high order solver for the data in a noisy empirical environment would be a very important step in our work. The smoothing of the input current density data or the weighted minimization of s by current density strength might be a couple of examples among many helpful tricks. Also it is very important to make an algorithm directly utilizing the magnetic field strength $\mathbf{B}$ or its z-component $\mathbf{B}_z$, instead of numerically differentiated values $\mathbf{J} = \nabla \times \mathbf{B}$ as in current standard $\mathbf{J}$-type MREIT technique [17, 20, 21]. We will discuss the nature of $\mathbf{B}$-type MREIT and possible numerical methods thoroughly in our future papers.

Acknowledgments

The work was supported by the Science/Engineering Research Center program of the Korea Science and Engineering Foundation (KOSEF) under grant number R11-2002-103. The author thanks an anonymous referee for pointing out that M Joy, A Nachman, K Hasanov, R Yoon and A Ma independently discovered the *curl-J* reconstruction formula (3.9) and sent an abstract of their technique to ISMRM recently.

References

[1] Birgül O, Eyüboglu B M and Ider Y Z 2003 Current constrained voltage scaled reconstruction (CCVSR) algorithm for MR-EIT and its performance with different probing current patterns *Phys. Med. Biol.* **48** 653–71

[2] Birgül O, Eyüboglu B M and Ider Y Z 2003 Experimental results for 2D magnetic resonance electrical impedance tomography (MR-EIT) using magnetic flux density in one direction *Phys. Med. Biol.* **48** 3485–504
[3] Borcea L 2002 Electrical impedance tomography *Inverse Problems* **18** R99–136
[4] Brühl M and Hanke M 2000 Numerical implementation of two noniterative methods for locating inclusions by impedance tomography *Inverse Problems* **16** 1029–42
[5] Gamba H R and Delpy D T 1998 Measurement of electrical current density distribution within the tissues of the head by magnetic resonance imaging *Med. Biol. Eng. Comput.* **36** 165–70
[6] Ider Y Z and Muftuler L T 1997 Measurement of ac magnetic field distribution using magnetic resonance imaging *IEEE Trans. Med. Imaging* **16** 617–22
[7] Ider Y Z, Onart S and Lionheart W 2003 Uniqueness and reconstruction in magnetic resonance electrical impedance tomography (MR-EIT) *Physiol. Meas.* **24** 591–604
[8] Khang H S, Lee B I, Oh S H, Woo E J, Lee S Y, Cho M H, Kwon O, Yoon J R and Seo J K 2002 *J*-substitution algorithm in magnetic resonance electrical impedance tomography (MREIT): phantom experiments for static resistivity images *IEEE Trans. Med. Imaging* **21** 695–702
[9] Kim S, Kwon O, Seo J K and Yoon J R 2002 On a nonlinear partial differential equation arising in magnetic resonance electrical impedance tomography *SIAM J. Math Anal.* **34** 511–26
[10] Kim Y J, Kwon O, Seo J and Woo E J 2003 Uniqueness and convergence of conductivity image reconstruction in magnetic resonance electrical impedance tomography *Inverse Problems* **19** 1213–25
[11] Kwon O, Lee J-Y and Yoon J R 2002 Equipotential line method for magnetic resonance electrical impedance tomography *Inverse Problems* **18** 1089–100
[12] Kwon O, Woo E, Yoon J R and Seo J K 2002 Magnetic resonance electrical impedance tomography (MREIT): simulation study of *J*-substitution algorithm *IEEE Trans. Biomed. Eng.* **49** 160–7
[13] Lee J Y and Yoon J R 2001 A numerical method for Cauchy problem using singular value decomposition *Commun. Korean Math. Soc.* **16** 487–508
[14] Lee B I, Oh S H, Woo E J, Lee S Y, Cho M H, Kwon O, Seo J-K and Baek W S 2003 Static resistivity image of a cubic saline phantom in magnetic resonance electrical impedance tomography (MREIT) *Physiol. Meas.* **24** 579–89
[15] Lee B I, Oh S H, Woo E J, Lee S Y, Cho M H, Kwon O, Seo J-K, Lee J-Y and Baek W S 2003 Three-dimensional forward solver and its performance analysis for magnetic resonance electrical impedance tomography (MREIT) using recessed electrodes *Phys. Med. Biol.* **48** 1971–86
[16] Mandache N 2001 Exponential instability in an inverse problem for the Schrodinger equation *Inverse Problems* **17** 1435–44
[17] Oh S H, Lee B I, Woo E J, Lee S Y, Cho M H, Kwon O and Seo J K 2003 Conductivity and current density image reconstruction using harmonic B_z algorithm in magnetic resonance electrical impedance tomography *Phys. Med. Biol.* **48** 3101–16
[18] Scott G C, Joy M L G, Armstrong R L and Henkelman R M 1991 Measurement of nonuniform current density by magnetic resonance *IEEE Trans. Med. Imaging* **10** 362–74
[19] Scott G C, Joy M L G, Armstrong R L and Henkelman R M 1995 Electromagnetic considerations for RF current density imaging *IEEE Trans. Med. Imaging* **14** 515–24
[20] Seo J K, Kwon O, Lee B I and Woo E J 2003 Reconstruction of current density distributions in axially symmetric cylindrical sections using one component of magnetic flux density: computer simulation study *Physiol. Meas.* **24** 565–77
[21] Seo J K, Yoon J-R, Woo E J and Kwon O 2003 Reconstruction of conductivity and current density images using only one component of magnetic field measurements *IEEE Trans. Biomed., Eng.* **50** 1121–4
[22] Woo E J, Lee S Y and Mun C W 1994 Impedance tomography using internal current density distribution measured by nuclear magnetic resonance *Proc. SPIE* **2299** 377–85
[23] Zhang N 1992 Electrical impedance tomography based on current density imaging *MSc Thesis* University of Toronto